Journal of Science and Technology in Civil Engineering NUCE 2018. 12 (3): 10–22

ANALYTICAL MODEL FOR PREDICTING MEMBRANE ACTIONS IN RC BEAM-SLAB STRUCTURES SUBJECTED TO PENULTIMATE-INTERNAL COLUMN LOSS SCENARIOS

Pham Xuan Dat[a,*], Trieska Yokhebed Wahyudi[b], Do Kim Anh[a]

[a] *Faculty of Building and Industrial Construction, National University of Civil Engineering, 55 Giai Phong road, Hai Ba Trung district, Hanoi, Vietnam*
[b] *Nanyang Technological University, Nanyang Avenue, 639798 Singapore*

Article history:
Received 15 March 2018, Revised 28 March 2018, Accepted 27 April 2018

Abstract

The potential for progressive collapse of RC buildings can be estimated by column loss scenarios. The loss of either internal or external penultimate columns is among the most critical scenarios since the beam-slab substructures associated with the removed column becomes laterally unrestrained with two discontinuous edges. At large deformations, membrane behaviour of the associated slabs, consisting of a compressive ring of concrete around its perimeter and tensile membrane action in the central region, represents an important line of defence against progressive collapse. The reserve capacity can be used to sustain amplified gravity loads and to mitigate the progressive collapse of building structures. In this paper, based on experimental observation of 1/4 scaled tests together with investigation of previous research works, an analytical model is proposed to predict the load-carrying capacity of beam-slab structures at large deformations. Comparison with the test results shows that the analytical model gives a good estimation of the overall load-carrying capacity of the RC slabs by membrane actions.

Keywords: Membrane actions; compressive ring; penultimate columns; load-carrying capacity; laterally unrestrained slab.

1. Introduction

It has been experimentally observed that the ultimate load of laterally unrestrained two-way reinforced concrete slabs is significantly higher compared with the capacity calculated by yield-line analysis [1–8]. The increase in the ultimate load is referred to as the contribution of membrane action which develops in slabs at large deformations. Membrane action in a laterally-unrestrained slab can be explained in Fig. 1. After the formation of yield lines, the slab is divided into four independent parts which are connected together by the yield lines. At large deformations the independent parts tend to move inwards under the action of increasing tensile forces at the centre of the slab, but are restrained from doing so by adjacent parts, creating a peripheral ring of compression supporting the

*Corresponding author. *E-mail address:* phamxdatcdc@gmail.com (Dat, P. X)

central net of tensile forces. The load-carrying capacity therefore comprises catenary action in the central region of the slabs and enhanced yield moment in the outer ring where in-plane compressive stresses occur.

The behaviour of laterally-unrestrained slabs at large deformations has been extensively studied by [3, 8–10]. It has been shown that the overall load-carrying capacity of membrane actions was at least twice the yield-line capacity. Recently, these mechanisms have been successfully applied to prevent the collapse of composite floors subjected to compartment fires in Europe through a simplified design method developed by [2].

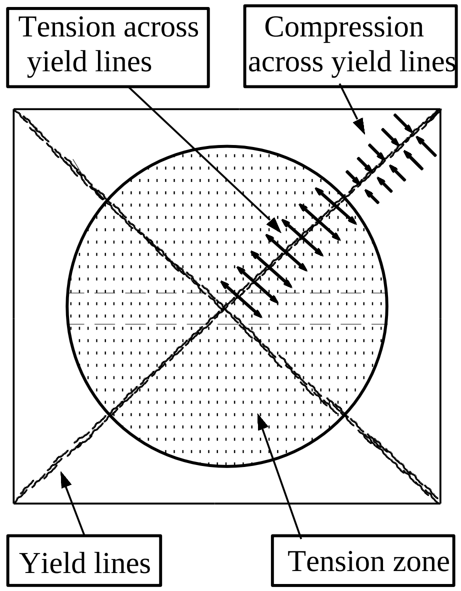

Figure 1. Membrane actions in a laterally unrestrained two-way slabs [1]

Nevertheless, most experimental and analytical works introduced so far are still limited in application, especially in terms of means to resist progressive collapse. The potential for progressive collapse of building structures can be estimated by column loss scenarios. The loss of a penultimate-internal column is among the most critical scenarios since the beam-slab structures associated with the lost column become laterally unrestrained with two discontinuous slab edges. As soon as the flexural action in beams fails to carry gravity loads which are amplified by both doubling-of-span and dynamic effects [11], the survival of the building structures totally depends on the strength of membrane actions developed in the affected slabs as indicated in Fig. 2(a). At floors above the first floor, if the stiffness and strength of their compressive rings are insufficient to support catenary action in the deflected central area, tension forces from catenary action may pull in the perimeter ground columns, leading to progressive collapse shown in Fig. 2(b). In this paper, an experimental programme and an analytical model to study the behaviour of

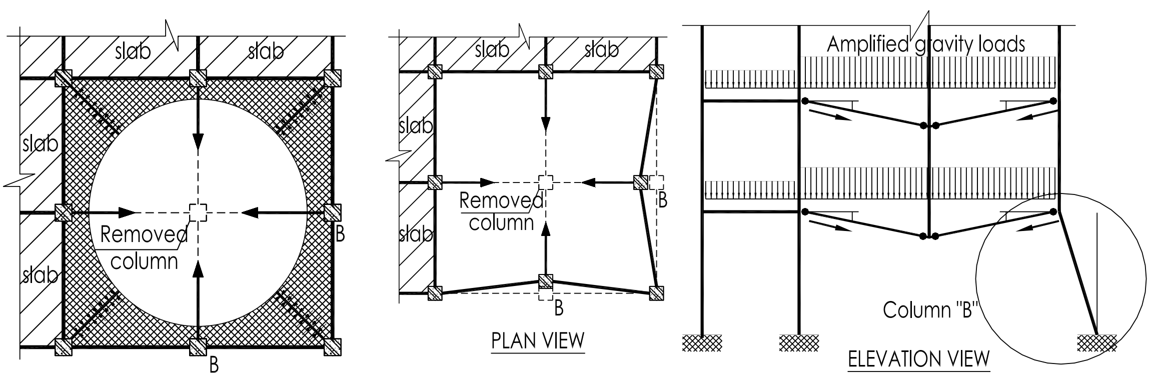

(a) Possible prevention by membrane actions

(b) Possible failure mode

Figure 2. Collapse of building structures under a Penultimate-Internal column loss [7]

membrane actions in RC beam-slab systems will be discussed. In the first part, the results of two ¼ scaled specimens which were constructed and tested under column loss scenario are presented.In the second part, a simplified method to predict the overall load-carrying capacity of beam-slab systems is discussed.

2. Experimental programme

2.1. Design

Two specimens have been designed, built and tested to investigate the tensile membrane action of RC building structures under a Penultimate-Internal (PI) column loss scenario. The dimensions of the test specimens are obtained by scaling down to ¼ dimensions of a prototype building designed for gravity loading. The design live load is 3 kN/m^2 and the imposed dead load is 2 kN/m^2. The detail of the test specimens can be summarized in Fig. 3 as well as Table 1.

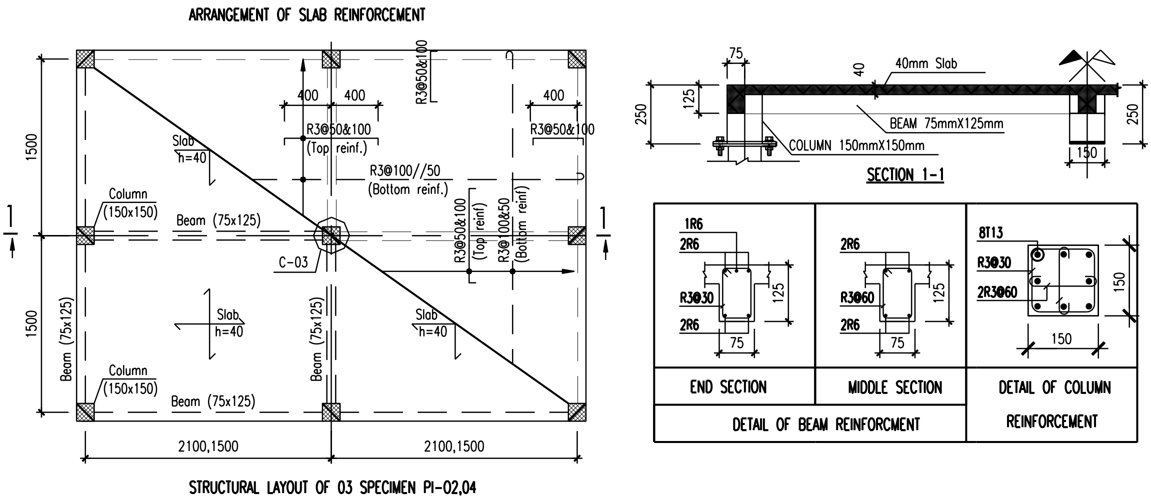

Figure 3. Detail of a typical specimen [12]

Table 1. Summary on test specimens [12]

	Overall dimension (Aspect ratio)	Top slab reinforcement	Bottom slab reinforcement along X-direction	Bottom slab reinforcement along Y-direction	Notes
PI-02	3000 × 4200 (a = 1.4)	Φ3 at 50 (ρ = 0.44%)	Φ3 at 100 (ρ = 0.22%)	Φ3 at 100 (ρ = 0.22%)	Isotropically reinforced
PI-04	3000 × 3000 (a = 1.0)	Φ3 at 100 (ρ = 0.22%)	Φ3 at 100 (ρ = 0.22%)	Φ3 at 50 (ρ = 0.44%)	Orthotropically reinforced

2.2. Material properties

Since the test specimens are scaled down by ¼ from the prototype building, the diameter of reinforcing bars is also scaled down by a certain factor so that the reinforcement ratios in beams, slabs and columns of the specimens can be kept approximately the same as those of the prototype structure. The plain round mild steel bar of 3 mm in diameter, R3, is used for slab reinforcement. The beams of the sub-assemblages are reinforced with R6, and the columns with 10 mm deformed bar (T10). In both beams and columns, R3 is used as transverse reinforcement. The nominal yield strength of round bars and deformed bars is 320 N/mm^2 and 460 N/mm^2, respectively. The concrete used in the test specimen was a small-aggregate mix with a characteristic design strength of 30 MPa. Due to the small thickness of slab (40 mm), chippings of 5 mm are used instead of normal-size aggregate to prevent any congestion and honey combs due to inadequate compaction. The concrete compressive test results are shown in Table 2.

Table 2. Concrete compression test results [12]

Sample No.	Weight (g)	Max. Load (kN)	Cylinder Strength (MPa)
1	11393	499.9	28.3
2	11505	615.9	34.9
3	11407	478.8	27.1
4	11414	436.2	24.7
5	11820	621.4	35.2
6	11531	482.5	27.3
Average	11512	528.9	29.6

2.3. Boundary condition

Under penultimate column loss condition, the affected beam-slab substructures behave as laterally unrestrained due to two consecutive discontinuous edges. Along the perimeter beams, however, the beam-column joints are rotationally restrained by the perimeter columns. Therefore, a set of 8 perimeter columns with one end pinned is designed to reasonably simulate the laterally yet rotationally restrained boundary condition. As shown in Fig. 4, the pin-ended columns allow the perimeter edges of specimens to move horizontally without any degree of restraint. The lateral reaction at the pin connection may provide perimeter beam-column joints with sufficient rotational restraint.

2.4. Loading method

With a special emphasis on a uniformly distributed load applied onto the beam-slab substructures under column loss condition, a loading scheme is designed based on existing laboratory constraints to reasonably simulate the applied loads in a uniform manner. A 200-ton actuator held by a reaction steel frame across the specimen is used to load the specimens to failure. The load from the actuator is distributed equally to twelve point loads (Fig. 5(a)) by means of loading trees (Fig. 5(b)). Ball and socket joints between steel plates and steel rods are used to keep the loading system as vertical as possible when the test specimens deform excessively.

Finite element analysis (FEA) is employed to investigate the accuracy of the loading method. The very small discrepancies of numerical predictions between the two cases indicate the reliability of the loading method. Fig. 6(a) shows the numerical models of square specimens with a plan dimension of 3 m$\times$3 m subjected to either uniformly distributed load of 1 kN/m^2 or 12 point loads of 0.75 kN. The very small discrepancies of numerical results (bending moment diagram shown in Fig. 6(b)) between

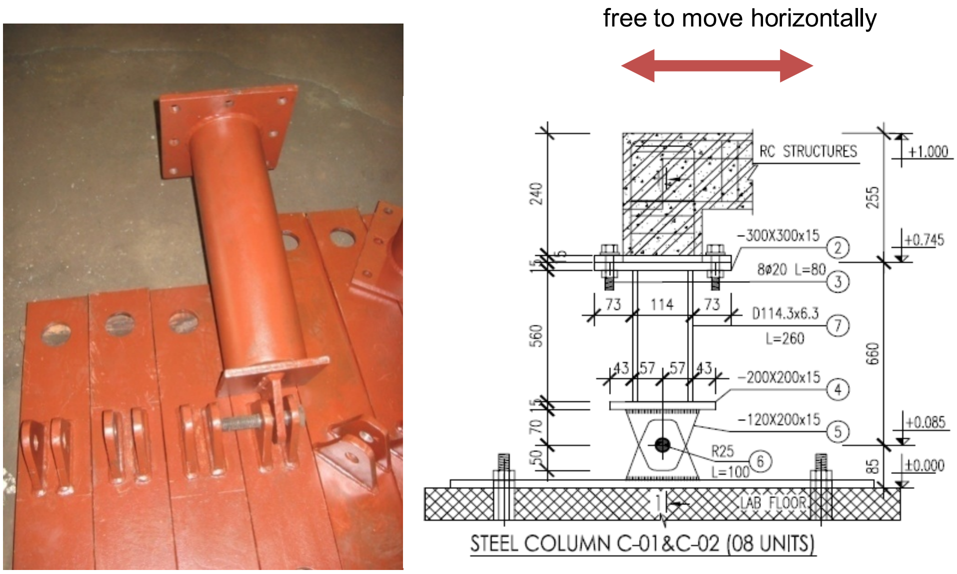

Figure 4. Supports and boundary condition [7]

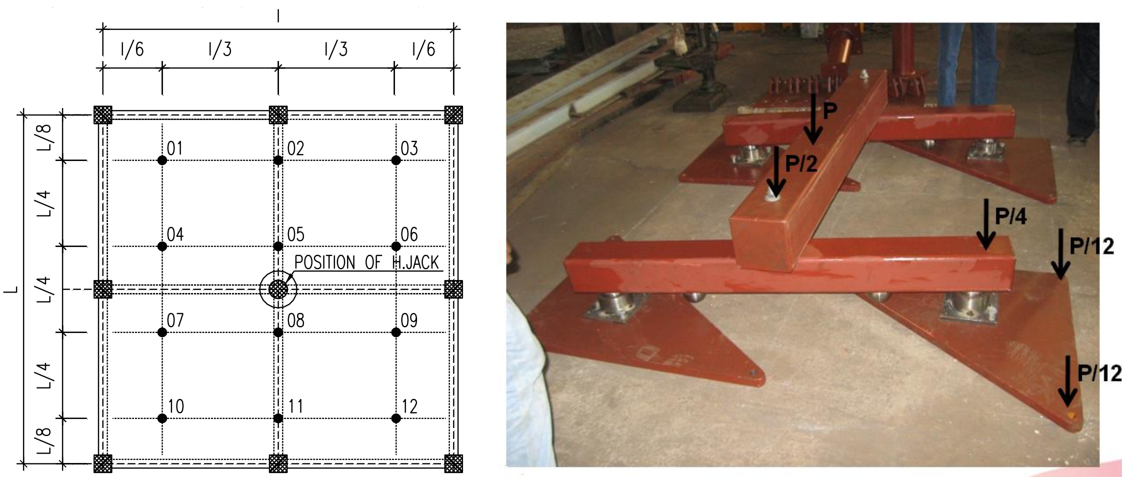

(a) Locations of 12 loading positions

(b) Loading tree system

Figure 5. Loading system for PI series specimens [7]

the two cases shown in Table 3 and Figs. 6 indicated the reliability of the loading method. Slightly better accuracy was obtained for the rectangular specimens

2.5. Instrumentation

The test specimens are installed or mounted with measuring devices both internally and externally (Fig. 7). The concentrated loads by the actuator are measured by using an in-built load cell which is connected in series with the actuator. Vertical reaction forces and moments in eight supporting columns can be calculated through four strain gauges (SG-1,2,3,4) mounted on the opposing external surfaces of the columns as shown in Fig. 7(a). At section where strain gauges are mounted, the axial

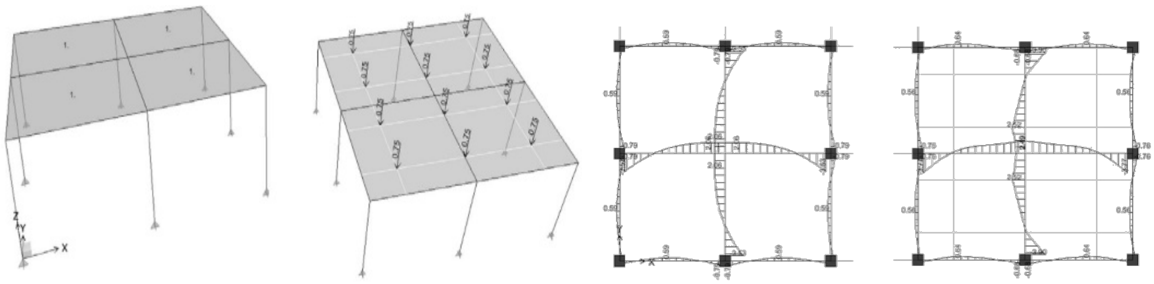

(a) A uniform load of 1 kN/m^2 Numerical model of specimens (b) Equivalent set of 12 point loads of 0.75 kN

Figure 6. Bending moment diagram in the two loading cases [7]

Table 3. Comparison of the numerical results between the two loading cases [7]

	Uniform load	12 point loads	Error
Central displacement	5.37 mm	5.66 mm	5.4 %
Axial force in edge columns	18.0 kN	18.2 kN	1.1%
Axial force in corner column	4.5 kN	4.2 kN	6.7%

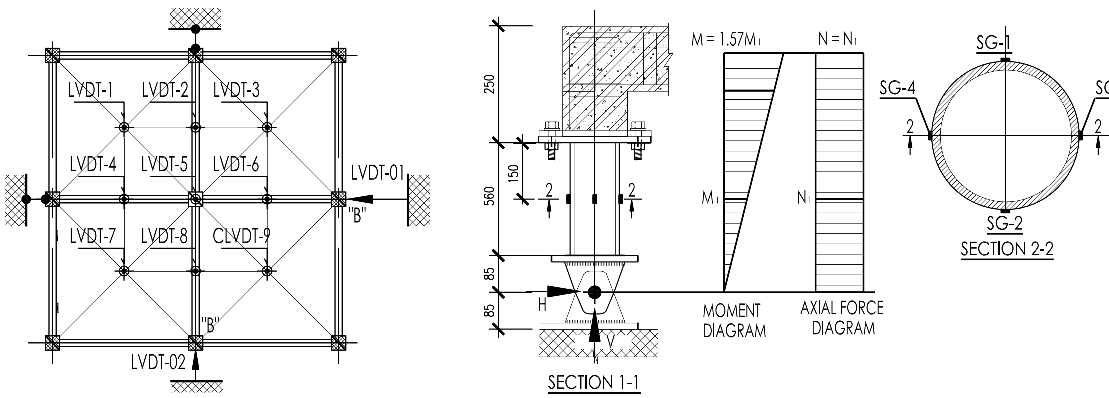

(a) Arrangement of LVDTs (b) Evaluation of reaction forces by strain gauges

Figure 7. External instrumentations [7]

forces N_1 and moments M_1 indicated in Fig. 7(b) can be evaluated by steel strains and cross-sectional properties as follows:

$$N_1 = E_{steel} * A_s * (\varepsilon_1 + \varepsilon_2 + \varepsilon_3 + \varepsilon_4)/4$$

$$M_1 = (E_{steel} * I * (\varepsilon_3 - \varepsilon_{ave}))/R\varepsilon_{ave} = (\varepsilon_1 + \varepsilon_2 + \varepsilon_3 + \varepsilon_4)/4$$

where E_{steel}, I, A_s, and R are elastic modulus of steel, moment of inertia, area, and radius of the hollow section, respectively ε_1, ε_2, ε_3, ε_4, ε_{ave} are the values recorded by SG-1,2,3,4 and average value of SGs-1,2,3,4.The reactions and the total moment of beam-column joint can be evaluated based on the diagrams illustrated in Fig. 7(b).

Vertical deformations of the test specimens were measured by nine Linear Variable Differential

Transducers (LVDT) (LVDT-1,2,3,4,5,6,7,8,9), as shown in Fig. 7(a). Readings from LVDT-5 was used to construct the load-displacement curve and the history of bending moments measured in supporting columns. Lateral deformations of the test specimen in x- and y- directions were measured by two other transducers installed on the top of columns: LVDT-01, 02. It was expected that these deformations may affect significantly the development of the peripheral compressive ring, and that of catenary action in the central region.

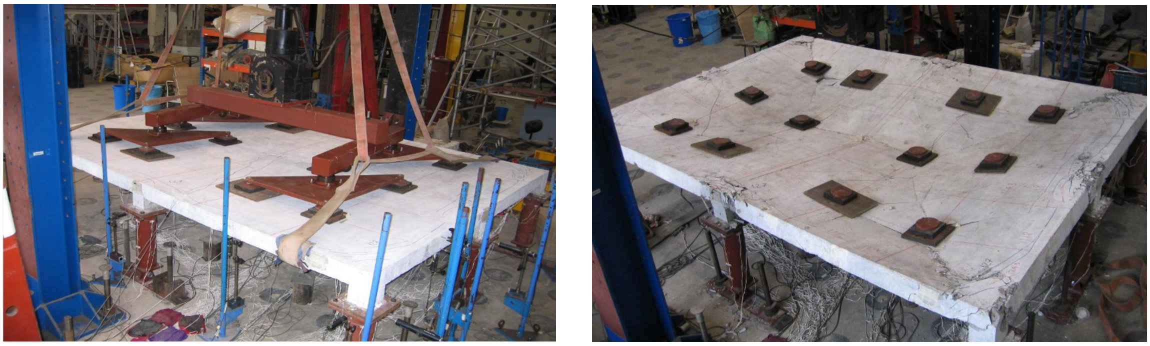

(a) Before the test

(b) After the test

Figure 8. Specimen PI-02 before and after the test [12]

Two specimens PI-02 and PI-04 are loaded to failure by the displacement-controlled procedure with two loading steps. In the initial stage, the specimens are statically loaded with a loading step of 1 mm. After the vertical central displacement reaches 50 mm, the loading step is increased to 2 mm toward the failure. Pure tensile membrane action in the central region which is defined by the presence of tensile strain at the top surface of slab is observed in the two tests at a central displacement of about 40 mm, one depth of RC slabs. As the displacement increases, the central tension region expands significantly, resulting in huge in-plan bending moments throughout the specimens.

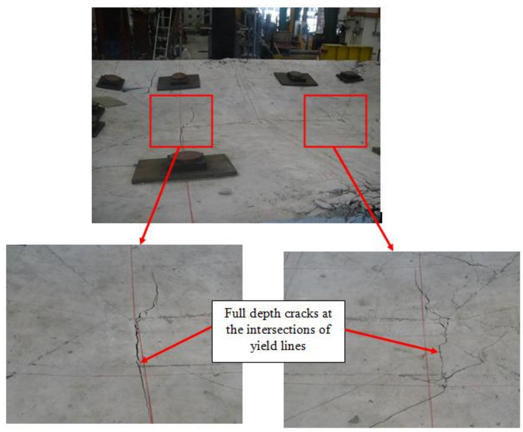

Figure 9. Failure mode of Specimen PI-02 [12]

Failure mode is the most important experimental observation as it is used to propose an analytical model for predicting the overall load-carrying capacity of the laterally-unrestrained beam-slab structure under a column loss scenario. With a relatively low slab reinforcement ratio of 0.2%, the failure of compressive ring due to concrete crushing does not occur in the two specimens. However, the failure mode appears at the final stage with two full-depth cracks together with bar fractures of slabs and interior beams at the intersections of yield-lines. This failure mode can be observed very clearly in Specimen PI-02 demonstrated in Figs. 8 and 9. In combination with the horizontal movement of unrestrained edges, it is possible that the final failure is due to in-plane bending moment along the long span.

3. Analytical model

Compared to the analysis of a simply supported slab, analysis of a beam-and-slab substructure requires three additional factors to be considered as follows: Rotational restraint along the perimeter edges of the slab; Two interior beams in the centre line; and Top reinforcement along the interior beams at the centrelines of the slab. It is predicted that the enhancement of load-carrying capacity in the beam-and-slab substructure is greater than that of the simply supported slab due to these factors. As more reinforcement is provided in the slab, the development of membrane action is more significant and the load-carrying capacity of RC slab is greater. A laterally-unrestrained slab at large deflection forms a self-equilibrating mechanism with compressive membrane forces at the outer ring and tensile membrane forces in the central region indicated in Fig. 10. Assuming rigid-plastic behaviour and simplifying the stress distribution into rectangular stress block, in Fig. 10. Assuming rigid-plastic behaviour and simplifying the stress distribution into rectangular stress block,the variation of membrane stresses along the yield lines can be simplified into in-plane stress distribution in Fig. 10. Considering equilibrium of Element 1 results in Eq (1),

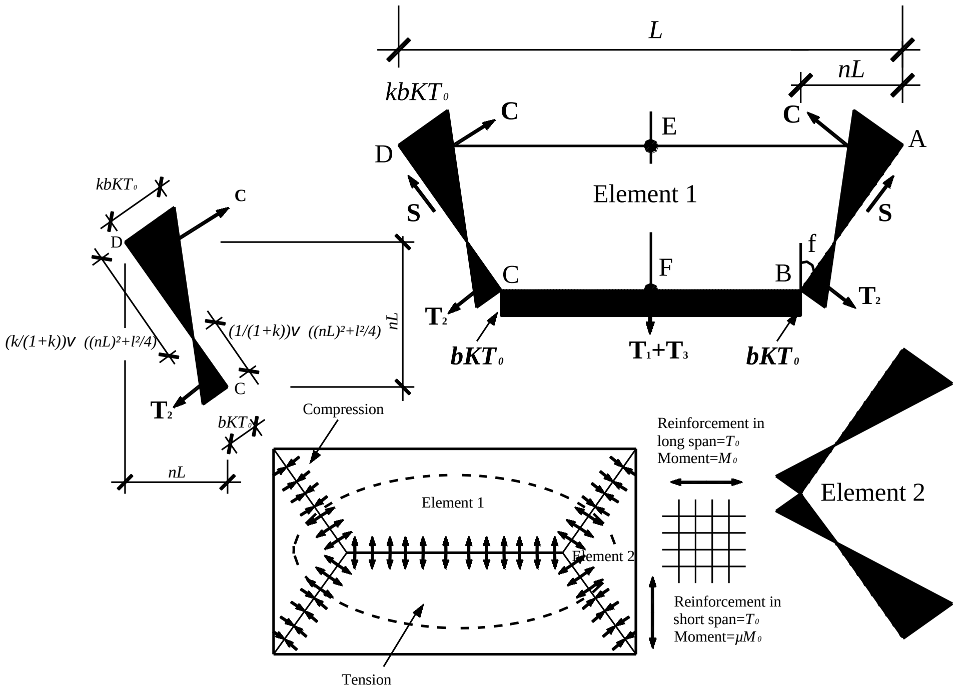

Figure 10. Assumed in-plane membrane forces [1, 2]

$$\frac{T_1 + T_3}{2} \sin\phi = (C - T_2) \tag{1}$$

$$T_1 = bK(T_{0,top} + T_{0,bot})(L - 2nL) \tag{2}$$

$$T_2 = \frac{bKT_{0,bot}}{2}\left(\frac{1}{1+k}\right)\sqrt{(nL)^2 + \frac{l^2}{4}} \tag{3}$$

$$T_3 = T_{b,top} \tag{4}$$

$$C = \frac{kbKT_{0,bot}}{2}\left(\frac{1}{1+k}\right)\sqrt{(nL)^2 + \frac{l^2}{4}} \tag{5}$$

$$S = \frac{1}{\tan\varphi}\frac{bKT_{0,bot}}{2}\sqrt{(nL)^2 + \frac{l^2}{4}(k-1)} \tag{6}$$

$$\sin\phi = \frac{nL}{\sqrt{(nL)^2 + \frac{l^2}{4}}} \tag{7}$$

From Fig. 10, there are Eqs. (2)–(7), where L: largest span of rectangular slab; l: shortest span of rectangular slab; b: parameter defining magnitude of membrane force; k: parameter defining magnitude of membrane force; n: parameter defining yield line; φ: angle defining yield-line pattern; $KT_{0,top}$: force in top steel per unit width in the shorter span; $KT_{0,bot}$: force in bottom steel per unit width in the shorter span. $T_{b,top}$: force in top interior beam steel.

Substituting into Eq. (1) gives Eq. (8),

$$k = 1 + \frac{4na^2(1-2n)}{1+4n^2a^2} \tag{8}$$

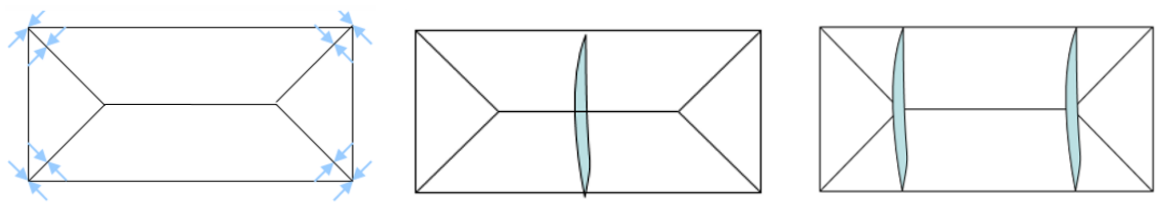

(a) Failure Mode 1 [2] Concrete compresion failure in the corner of the slab

(b) Failure Mode 2 [1] Fracture of reinforcement across the centre of slab

(c) Failure Mode 3 [1] Fracture of reinforcement across the intersection of yield lines

Figure 11. Three possible failure modes

The magnitude of parameter k can be obtained through Eq. (8). The value of parameter b can be obtained by considering the failure modes of slab. Depending on how and where the critical section is formed, there are three possible failure modes of the slab at the TMA stage shown in Fig. 11 [1, 2]. The typical failure modes are indicated by formation of large cracks across the shorter span of the slab resulting in the fracture of the reinforcement as in Fig. 11(b) and 11(c). Nevertheless, recent test by Bailey et al [2] showed that compression failure due to large in-plane compressive force at the slab perimeter edge can also be counted as another possible mode of failure indicated in Fig. 11(a).

Failure Mode 1

If large in-plane compressive forces at the slab perimeter edge govern the slab failure, the magnitude of membrane forces which are reflected by parameter b can be determined from equilibrium of slab edge section Assuming that the maximum depth of the compressive stress block is limited to 0.45 of average effective depth, the following equation can be obtained Eq (9),

$$b = \frac{1}{kKT_o}\left(0.67f_{cu}0.45\left(\frac{d_1+d_2}{2}\right) - T_0\left(\frac{K+1}{2}\right)\right) \tag{9}$$

where d_1: effective depth of reinforcement in shorter span; d_2: effective depth of reinforcement in longer span; KT: force in steel per unit width in the shorter span; T: force in steel per unit width in the longer span; f_{cu}: compressive cube strength.

To predict the magnitudes of membrane forces in failure mode 2, a free body diagram as shown in Fig. 12 is analyzed. It is assumed that all reinforcement along the critical section (line EF) is at ultimate stress, which is approximately 10 percent greater than the yield stress. According to Hayes [3], this is a reasonable assumption since the mode of failure is by fracture of reinforcement Hence, taking moment about E gives

$$b = \frac{[1.1l^2K(T_{0,top} + T_{0,bot})/8 + 1.1T_3 l/2]/K}{\left(AT_{0,bot} + BT_{0,bot} + CT_{0,bot} - D(T_{0,top} + T_{0,bot})\right)} \tag{10}$$

The derivation for parameter b in failure mode 3 is also introduced by analyzing the free body diagram of the critical section in the slab. Since the critical section is assumed to be at the intersection of yield lines, the free body diagram will be as shown in Fig. 13.

$$b = \frac{(1 + k)(3.3T_{0,bot} + 13.2T_3/l)}{KT_0[3k^2 + 4n^2a^2(2k^2 + k - 1)]} \tag{11}$$

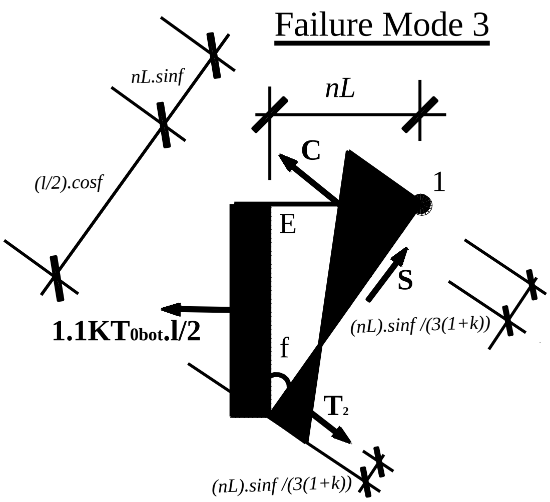

Figure 12. Analysis of membrane action in failure mode 2 for RC beam-slab structure [1]

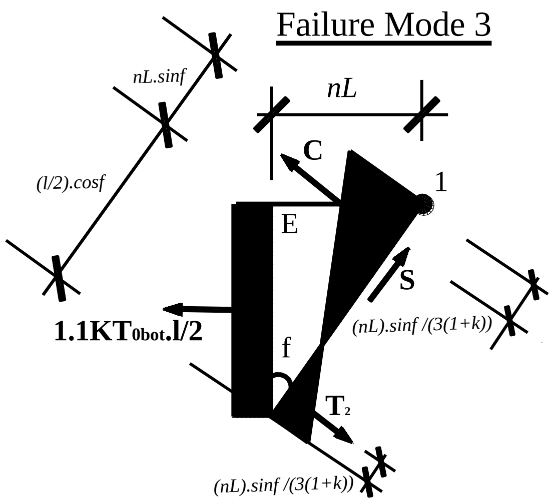

Figure 13. Analysis of membrane action in failure mode 3 for RC beam-slab structure [1, 2]

where A, B, C, and D are defined as follows. The detailed derivation of Eqs. (1), (9), (10), (11) can be found in reference [1, 2]. After the parameter b for all possible failure modes has been obtained, the correct failure mode can be determined. Since this is an upper bound or an unsafe approach, the failure mode that gives the smallest b is deemed to be the correct failure mode. Table 4 shows the comparison between parameter b obtained from the three possible failure modes. It can be concluded that failure mode 3 is the correct failure mechanism as it gives the smallest parameter, b, for both specimens. This is in line with the test results of Specimen PI-02, as shown in Fig. 9.

$$A = \frac{1}{2}\left(\frac{1}{1+k}\right)\left[\frac{l^2}{8n} - \frac{(L/2 - nL}{nL}\left((nL)^2 + \frac{l^2}{4}\right) - \frac{1}{3}\left(\frac{1}{1+k}\right)\left((nL)^2 + \frac{l^2}{4}\right)\right], \quad C = \frac{l^2}{16n}(k-1)$$

$$B = \frac{1}{2}\left(\frac{k^2}{1+k}\right)\left[\frac{nL^2}{2} - \frac{k}{3(1+k)}\left((nL)^2 + \frac{l^2}{4}\right)\right], \quad D = \left(\frac{L}{2} - nL\right)\left(\frac{L}{4} - \frac{nL}{2}\right)$$

Table 4. Comparison of parameter b

Specimen	Failure Mode		
	1	2	3
PI-02	9.53	5.32	2.07
PI-04	11.30	5.20	4.70

Once the membrane forces are defined, the corresponding load-carrying capacity of slabs by means of enhancement factor can be calculated. The contribution of membrane forces and the increase in bending resistance in enhancing the load-carrying capacity of the slab are calculated using Eq. (12)

$$e = (e_{1m} + e_{1b}) - \frac{(e_{1m} + e_{1b}) - (e_{2m} + e_{2b})}{1 + 2\mu a^2} \tag{12}$$

The subscript "m" and "b" in above Eq. (12) denote the enhancement in load-carrying capacity due to membrane forces and increase in bending resistance, respectively. On the other hand, the subscript "1" and "2" in the Eq. (12) indicate the enhancement from element 1 (the trapezoid section) and element 2 (the triangular section) of the slabs in Fig. 10, respectively. The detailed derivation of Eq. (12) can be found in references [1, 2].

Since the enhancement factor obtained by using Eq. (12) is originally derived for the case of a simply supported slab, the factor cannot be readily used to calculate the increase of load-carrying capacity of RC beam-slab structure. Instead, the enhancement factor can only be applied to the load-carrying capacity of positive yield line of RC beam-slab structure. The load-carrying contribution from the negative yield line is initially assumed to remain constant after yielding. Nevertheless, as observed during the test, concrete crushing at the bottom face of interior beam-column joints (Fig. 14) cause the bottom face of concrete to flake off and reduce the effective depth (d) and the negative beam and slab moment capacity of the section ($M_{beam,neg}$ & m_{sneg}). Hence, as deflection increases, the load-carrying contribution from the negative yield line is not constant, but decreasing. This phenomenon is also reflected in the variation of column bending moments during the test as shown in Fig. 15. Hence, it can be assumed that the decreasing slope for negative yield line capacity at large deflection is the same as the decreasing slope of column moments (r) obtained during the tests.

Assuming that the total load-carrying capacity (P_{tot}) of the slab is equal to the linear summation of the positive yield line load (P_{pos}) and the negative yield line load (P_{neg}), the total load-carrying capacity of the RC beam-slab structure can be expressed mathematically as Eq. (13). While the enhancement factor (e) can be obtained analytically, the reduction factor (r) is obtained empirically. Hence, the simple method to predict the load-deflection relationship at TMA stage becomes semi-empirical.

$$P_{tot} = e \times P_{pos} + r \times P_{neg} \tag{13}$$

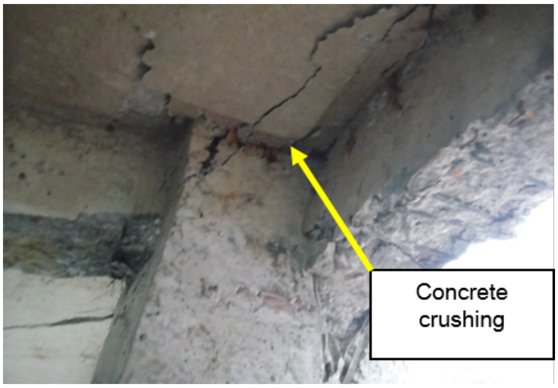

Figure 14. Concrete crushing at the bottom face of beam-column joint [12]

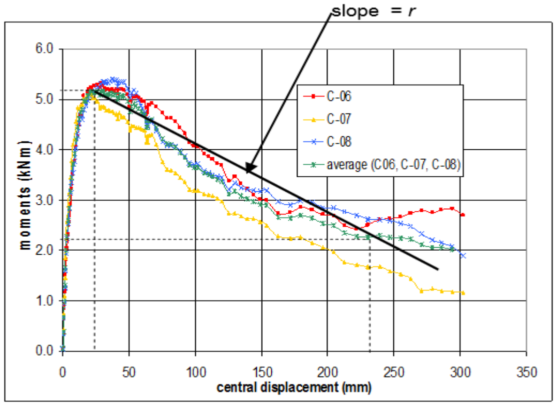

Figure 15. Declining trend of bending in columns [12]

4. Validation of the analytical model with the experimental results

Fig. 16 and Fig. 17 show the load-deflection curves obtained from both the test results and the analytical model for Specimen PI-02 and PI-04, respectively. Since the semi-analytical model is based on rigid, perfectly plastic behaviour, it is not intended to predict the elastic and elastic-plastic behaviour at the initial stage of the tests. It can be seen from both figures that at large deformation, the semi-analytical model produces good agreement with the tests results.

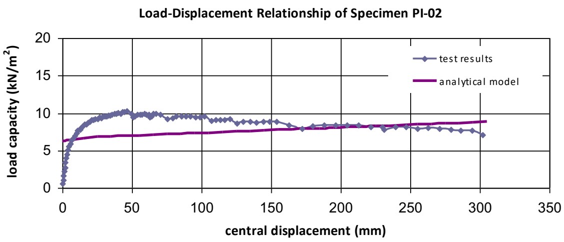

Figure 16. Comparison between test results and analytical model for Specimen PI-02 [12]

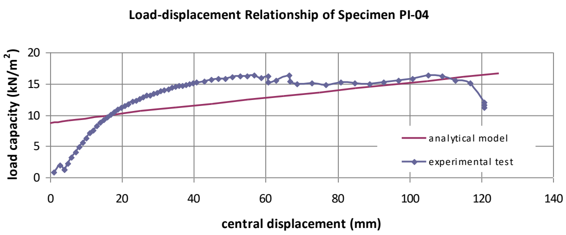

Figure 17. Comparison between test results and analytical model for Specimen PI-04 [12]

5. Conclusion and future works

A new model to estimate the load-deflection relationship of laterally-unrestrained RC beam-slab structure at TMA stage has been proposed. The model predicts that the slabs will fail due to fracture of reinforcement along the intersection of yield lines, which is similar to the failure mechanism observed in the tests. Comparison with the test results also shows that the semi-analytical model gives a very good estimation of the overall load-carrying capacity of RC slabs at large deflections. However, the number of experiments was slightly less (only two samples in this article).

Nevertheless, the simple model to predict the behaviour of RC beam-slab structure at TMA stage presented in this paper has not yet been extended to incorporate the decreasing negative yield line capacity analytically. In addition, a safe maximum value for the central displacement can be further determined. Finally, the experimental tests together with the simple analysis presented in this paper are designed to address the internal penultimate column loss scenario. The effectiveness of TMA under external penultimate column loss scenario should be further investigated. Also study more about numerical simulation and research by other authors to verify the analytical model.

Acknowledgements

The study presented in this paper was financially supported by National Foundation For Science and Technology Development (NAFOSTED), Vietnam through Grant #107.01-2016.07. The financial support is greatly appreciated. The authors would like to thank Professor Tan Kang Hai (NTU, Singapore) for his helpful comments on this paper.

References

[1] Bailey, C. G. (2001). Membrane action of unrestrained lightly reinforced concrete slabs at large displacements. *Engineering Structures*, 23(5):470–483.

[2] Bailey, C. G., Toh, W. S., and Chan, B. M. (2008). Simplified and advanced analysis of membrane action of concrete slabs. *ACI Structural Journal*, 105(1):30–40.

[3] Hayes, B. (1968). Allowing for membrane action in the plastic analysis of rectangular reinforced concrete slabs. *Magazine of Concrete Research*, 20(65):205–212.

[4] Kemp, K. O. (1967). Yield of a square reinforced concrete slab on simple supports, allowing for membrane forces. *The Structural Engineer*, 45(7):235–240.

[5] Park, R. and Gamble, W. L. (1998). *Reinforced concrete slabs*. John Wiley & Sons.

[6] Park, R. (1964). Tensile membrane behaviour of uniformly loaded rectangular reinforced concrete slabs with fully restrained edges. *Magazine of Concrete Research*, 16(46):39–44.

[7] Pham, X. D. (2009). *Tensile membrane action in preventing progressive collapse of RC building structure subjected to a column removal*. PhD First Year Report, Nanyang Technological University, Singapore.

[8] Sawczuk, A. and Winnicki, L. (1965). Plastic behavior of simply supported reinforced concrete plates at moderately large deflections. *International Journal of Solids and Structures*, 1(1):97–111.

[9] Brotchie, J. F. and Holley, M. J. (1971). Membrane action in slabs. *International Symposium on the Cracking, Deflection, and Ultimate Load of Concrete Slab Systems - American Concrete Institute*, 30: 345–377.

[10] Mitchell, D. and Cook, W. D. (1984). Preventing progressive collapse of slab structures. *Journal of Structural Engineering*, 110(7):1513–1532.

[11] Sasani, M., Bazan, M., and Sagiroglu, S. (2007). Experimental and analytical progressive collapse evaluation of actual reinforced concrete structure. *ACI Structural Journal*, 104(6):731–739.

[12] Wahyudi, T. Y. (2010). *Tensile membrane action at reinforced concrete slabs*. Final Year Report, School of Civil and Environmental Engineering, Nanyang Technological University.